IPEM Institute of Physics and Engineering in Medicine

PAPER • OPEN ACCESS

Systematic quantification of nanoscopic dose enhancement of gold nanoparticles in ion beams

View the article online for updates and enhancements.
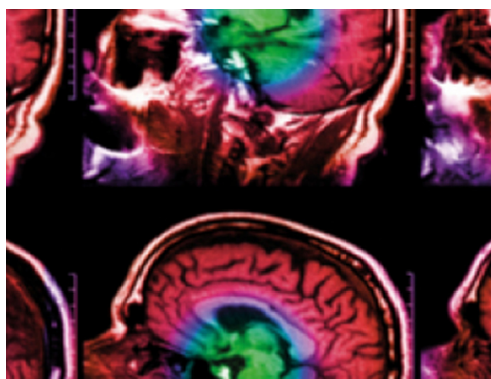
IPEM | IOP

Series in Physics and Engineering in Medicine and Biology

Your publishing choice in medical physics, biomedical engineering and related subjects.

Start exploring the collection–download the first chapter of every title for free.

Physics in Medicine & Biology

IPEM Institute of Physics and Engineering in Medicine

Systematic quantification of nanoscopic dose enhancement of gold nanoparticles in ion beams

M C Fuss[1] , D Boscolo[1] , M Durante[1,2] , E Scifoni[3] and M Krämer[1]

[1] GSI Helmholtzzentrum für Schwerionenforschung GmbH, Planckstraße 1, 64291 Darmstadt, Germany
[2] Technische Universität Darmstadt, Hochschulstraße 6, 64289 Darmstadt, Germany
[3] Trento Institute for Fundamental Physics and Applications (TIFPA), National Institute for Nuclear Physics (INFN), Via Sommarive 14, 38123 Trento, Italy

E-mail: m.fuss@gsi.de

Abstract

High-Z material nanoparticles are being studied as localized dose enhancers in radiotherapeutic applications. Here, the nano-scale physical dose enhancement of proton, carbon and oxygen ion beam radiation by gold nanoparticles was studied by means of Monte Carlo track structure simulation with the TRAX code. We present 2D distributions and radial profiles of the additional dose and the dose enhancement factor for two geometries which consider an isolated and a water-embedded nanoparticle, respectively. Different nanoparticle sizes (radius of 1.2–22 nm) were found to yield qualitatively different absolute and relative dose enhancement distributions and different maximum dose enhancement factors (up to 20). Whereas the smallest nanoparticles produced the highest local dose enhancement factor close to the metal, larger ones led to lower, more diffuse dose enhancement factors that contributed more at larger distances. Differential absorption effects inside the metal were found to be responsible for those characteristics. For the energy range 15–204 MeVu^{-1}, also a mild trend with ion E/A, regardless of the ion species, was found for embedded nanoparticles. In analogy to the width of the ion track itself, slower ions increased the enhancement at the nanoparticle surface. In contrast, no dependence on linear energy transfer was encountered. For slower ions (3–10 MeVu^{-1}), the enhancement effect began to break down over all distances. Finally, the significance of any indirect physical effect was excluded, giving important hints especially in view of the low probabilities (at realistic concentrations and fluences) of direct ion-NP-hits. The very localized nature of the physical dose enhancement found suggests a strong action upon targets closeby, but no relevant effect at cellular distances. When pondering different possible damage enhancement mechanisms of gold nanoparticles in the context of published *in vitro* and *in vivo* experimental results, biological pathways are likely to play the key role.

1. Introduction

Following the seminal work of Matsudaira *et al* (1980), Herold *et al* (2000) and Hainfeld *et al* (2004), a large interest has been attracted by the possibility of using high-Z nanoparticles (NPs) for radiation enhancement in radiotherapeutic applications. They are already widely used as contrast agents in diagnostic applications, exploiting that they accumulate preferentially in tumours due to the enhanced permeability and retention (EPR) effect. They could, hence, enable simultaneous imaging and therapy sessions in 'theranostic' applications. The basic physical advantage of those heavy atom materials resides in the much higher interaction probability and thus an increased emission of secondary radiation that deposits an additional dose locally. Depending on the primary radiation type and energy range, different mechanisms contribute and yield different spectra of secondaries. Photons in the keV range exhibit a highly enhanced cross section

for photoelectric effect in heavy elements as compared to low-Z biological tissue and their secondary electron spectrum effectively hardens upon scattering by metal NPs. Charged particles in turn have secondary spectra which peak around 50 eV–100 eV and display only a moderate dependence on the target material Z. Triggered by the initial physical interactions, one can expect the differences to translate to the indirect effect (mediated by radical production). A biologically enhanced effectiveness can result from physical dose enhancement or small-scale inhomogeneities, additional ROS production, a synergistic effect between cytotoxicity and radiation, and any combination thereof, with the respective contributions for each type of radiation and nanoparticle still under discussion.

Effective radioenhancement has been shown many times for photon beams (e.g. Chitrani *et al* 2010, Jain *et al* 2011, Xiao *et al* 2011, Butterworth *et al* 2013, Cui *et al* 2014) and is predicted, at least partially, by theoretical models (Jones *et al* 2010, Lin *et al* 2014, Ferrero *et al* 2017, Xie *et al* 2015, Delorme *et al* 2017). As a general trend, a more effective radiosensitization has been observed for keV photons than in the clinical MeV range experimentally (cf Chitrani *et al* 2010, Geng *et al* 2011) and in computational studies (Montenegro *et al* 2009, Lechtman *et al* 2011, Lin *et al* 2014), but for both energy ranges the experimental enhancement ratios are typically much higher than the calculated physical dose increase (Butterworth *et al* 2013) and thus point towards additional contributions by other mechanisms, as afore mentioned.

The sensitization effect that might be achieved for ion irradiation is the subject of ongoing investigations (for recent reviews, see Lacombe *et al* (2017), Peukert *et al* (2018), Kuncic and Lacombe (2018)) some of which have found encouraging results *in vitro* or *in vivo*. Protons have received particular attention and have been investigated in both experimental (Kim *et al* 2010, Polf *et al* 2011, Kim *et al* 2012, Jeynes *et al* 2014, Li *et al* 2016) and simulation (Wälzlein *et al* 2014b, Jeynes *et al* 2014, Lin *et al* 2014, Lin *et al* 2015, Martínez-Rovira and Prezado 2015, Tran *et al* 2016, Sotiropoulos *et al* 2017, Peukert *et al* 2019, Rudek *et al* 2019) studies. Among different metals, gold is one of the most studied candidates because of its known biological inertness and biocompatibility, at least macroscopically as a bulk material, and the straightforward synthesis and conjugation to appropriate coating molecules (Conde *et al* 2014).

In this article, we examine the physical dose enhancement effect caused at the nano-scale by gold nanoparticles in a water environment under proton, ^{12}C ion, and ^{16}O ion irradiation in two different geometries. We systematically model the impact of different energies (3–204 MeVu^{-1}) and nanoparticle sizes (radius R of 1.2–22 nm) on the spatial dose (enhancement) distribution. This parameter set is selected to cover beams representing the entrance channel (80 MeV protons, 108 MeVu^{-1} C ions and 204 MeVu^{-1} O ions), an intermediate depth, the target region (15 MeV protons, 42 MeVu^{-1} C ions and 27 MeVu^{-1} O ions), and finally a Bragg peak energy (3 MeVu^{-1}), and to include a range of NP sizes typically used in radiobiological experiments. In this way, we shed some light on general questions such as absorption in the metal, the specific impact of Auger electrons and the possibility of any indirect physical effect. By directly comparing three different ion species over a large energy range, possible dependencies on linear energy transfer (LET) can furthermore be uncovered.

2. Materials and methods

2.1. Monte Carlo track structure calculations

For the present simulations, the TRAX Monte Carlo code has been used (Krämer and Kraft 1994, Wälzlein *et al* 2014a). It is designed to track the passage of electrons and ions through different materials by simulating, event by event, each basic interaction and recording the individual positions and energy depositions of primary and secondary particles. Photons (that can originate from fluorescence or Bremsstrahlung) are currently not included in the model. However, the impact of PIXEs (particle induced x-ray emissions) on the presented results is expected to be negligible based on the argumentation of Dollinger (2011) and theoretical comparisons with / without photons by Tran *et al* (2016). TRAX offers a specialized series of evaluation routines and has built-in cross section calculation functions for atomic and certain molecular materials. Its modular design allows for both new interactions, particle types, and cross section (CS) tables to be easily incorporated. The energy range addressed by the code spans from a maximum energy of several hundred MeVu^{-1} for ions and about 1 MeV for electrons to a lower threshold of a few eV (depending on the material). In particular, the implementation of shell specific interaction cross sections allows the energy deposition process of secondary electrons to be described in detail down to the sub-electronic excitation region. Additionally, the molecular radiation damage caused in a water target by ionizations and specific excitations (water radiolysis) is also quantified and can be handed over to the pre-chemical and chemical stage model (Boscolo *et al* 2018, Boscolo *et al* 2020).

The cross sections used in the present article have been described in detail previously (Wälzlein *et al* 2014b, Boscolo 2018) and include the generation of Auger electrons and cascades and an extended evaluated

Figure 1. Simulation setups and reference cases used. (a,b) isolated NP, (c,d) embedded NP.
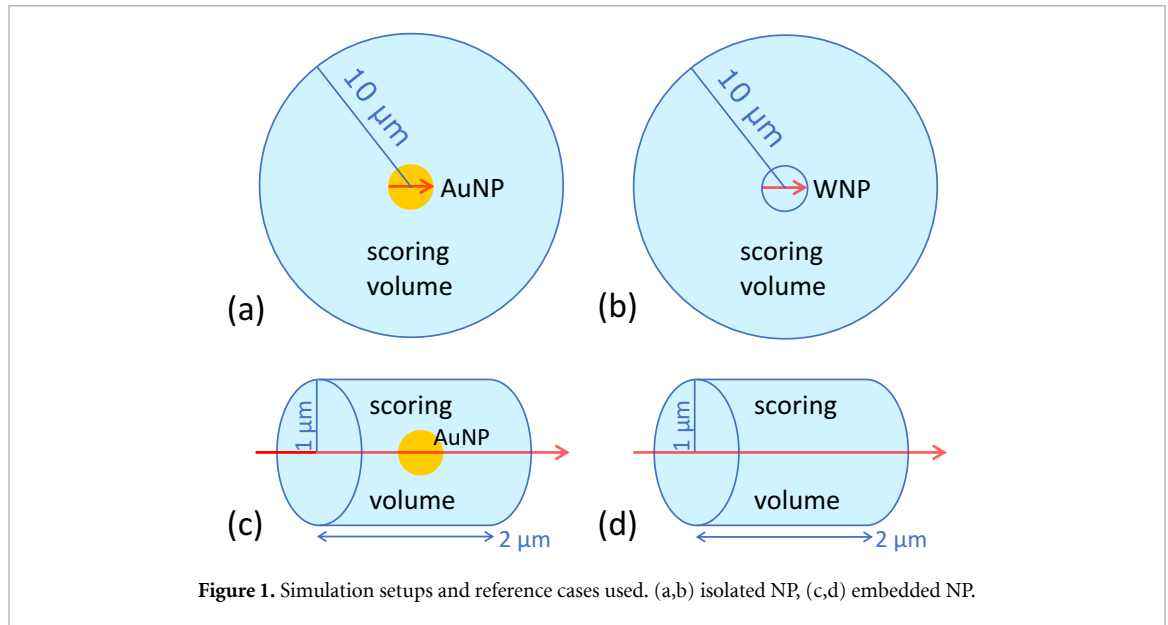
set of cross section data in Au (including the volume plasmon excitation). The surface plasmon excitation in the gold nanoparticles is not currently included. It would contribute mainly to the production of secondary electrons below the electronic excitation threshold of water (Verkhovtsev *et al* 2015), causing local dose deposits and adding a small portion of extra aqueous electrons to the chemical stage which is not simulated here. The validity of the TRAX model for gold has been recently confirmed by comparing experimental and simulated electron scattering from gold surfaces and NPs irradiated with protons and with a mixed β/γ spectrum (Hespeels *et al* 2017, Hespeels *et al* 2019a, Williart *et al* 2019). Due to the event-by-event simulation down to low energies (few eV) and the use of dedicated input data tables, TRAX is especially suited for studying the very localized, nanometric effects expected from the combination of heavy ion radiation with Au NPs.

2.2. Simulation geometries

The dose enhancement effect is studied for two different geometries: an 'isolated' and an 'embedded' nanoparticle. In the first case, a spherical 'isolated gold NP' subject to ion radiation is simulated and compared to a pure water volume of the same size and shape ('water NP', WNP) in analogy to Wälzlein *et al* (2014b). In this picture, an additional spherical water volume of 10 μm radius surrounds the NP in question to emulate the biological absorber where the radiation dose is deposited. As a matter of fact, in this geometry the primary (ion) interactions can only take place in the (gold or water) NP studied, while energy deposition —caused by secondary electrons— is scored in the surrounding water. This geometry is especially useful for isolating the pure effect of metal NP irradiation without any influence from the surroundings, and compare to the reference material, water. It has been used previously in different implementations e.g. by Tran *et al* (2016) and Hespeels *et al* (2019a) and can be useful for comparisons to other published results.

Our second approach is to subsequently include the radiation effect on the outer biological absorber by simulating an entire ion track in water and its traversal of a Au NP. Due to the cylindrical symmetry of the ion track and the respective data, the absorber volume was chosen to be a cylinder (1 μm radius, 2 μm length) and we refer to it as the 'embedded gold NP' and its pure water equivalent. The embedded geometry is the one that would be found in potential medical applications, where radiation is delivered externally through the surrounding biological tissue and a NP cannot be targeted selectively. This approach resembles the one used by Lin *et al* (2015). A sketch of both simulation setups adopted by us, with and without gold NP, is given in figure 1. Both cases assume an infinitesimal ion beam emitted by a point-like source and a central hit of the NP. Moreover, the simulation examples in both geometries generally satisfy track segment conditions, i.e. LET can be considered uniform. Deviations from this simplified case will be treated in section 3.4.

In order to quantify the differences found when including/excluding a gold NP, results are presented in terms of the *absolute dose deposition* and the *dose difference*. Additionally, the *dose enhancement factor* (DEF), defined as

$$\text{DEF} = \left. \frac{D_{\text{test}}}{D_{\text{reference}}} \right|_{\text{same irradiation conditions}}$$

and here applied as
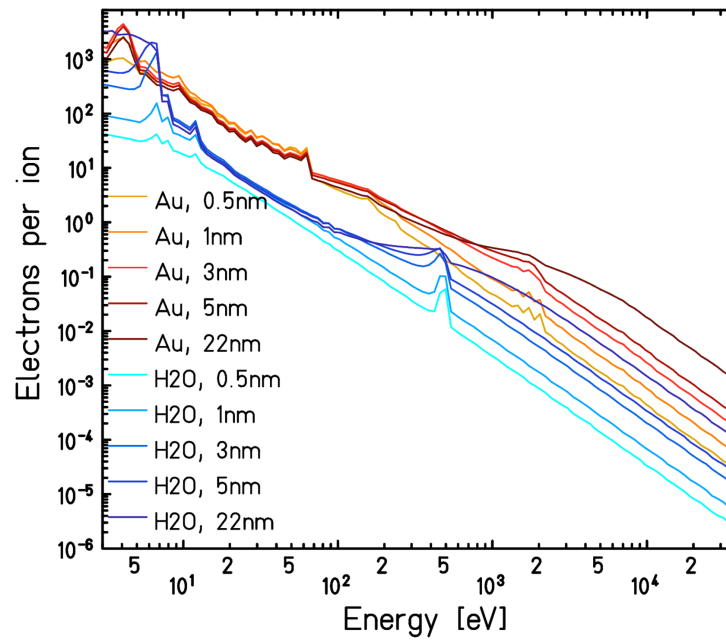
Figure 2. TRAX-simulated electron emission from different sizes of H_2O and Au nanoparticles for irradiation with 42 MeVu^{-1} C ions (average over between 10^7 and $2 \cdot 10^8$ histories).

$$\left. \frac{D_{\mathrm{AuNP}}}{D_{\mathrm{WNP}}} \right|_{\text{same irradiation conditions}},$$

has proven useful and is used throughout this paper. Note that for line profiles and spatial distributions, the DEF is calculated pointwise. Furthermore, in the present simulation cases dose distributions in the scoring volume are calculated based on the effective energy deposition per mass by all inelastic processes, not on the ionization frequency (which is more typical in experimental practice).

3. Results

3.1. Electron spectra emitted from gold and water

Since the physical effect of including metal NPs into a biological target results from the increased interaction cross section and, as a consequence, a higher emission of secondary particles, it is helpful to examine the electron emission spectra of isolated NPs of both materials (figure 2). In both cases, an energy-selective absorption was found in the low and intermediate energy range ($\lesssim 150$ eV) after increasing the NP radius from 0.5 nm up to 22 nm. Smaller/different sizes than in the following sections are used here in order to better highlight the self-absorption behaviour as a function of size. For the water NP, sizes > 3 nm failed to increase the absolute emission in the range 7–150 eV but rather cause a stabilization or small decrease. The electron emission between < 3 eV and 70 eV from Au NPs even drops continuously when increasing the NP size over 1 nm. This underlines the high probability of interaction of the abundant low energy electrons released by the ion, which eventually avoids their transport into the surrounding medium. The higher-energy part of the emission spectrum (≥ 200 eV for water and ≥ 1 keV for gold) did however present an effective increase for larger NPs. This arises because first, electrons in the keV range have a lower interaction cross section with either material and second, if interacting they have a higher range and can escape the NP more easily. Compared to the secondary emission of an ion in pure water, the Au NP has a hardening effect on the electron spectrum. In what follows, on various occasions, the differential absorption or emission for the two materials in the different energy ranges determines the final enhancement result and its variation with NP size.

3.2. Dose enhancement of an isolated NP

Calculated dose distributions caused by *isolated* gold and water nanoparticles (corresponding to figures 1(a) and (b)) were found to be spherically symmetric in good approximation, with only a slight increase perpendicular to the incident beam direction for the pure water case and localized dose peaks at the ion entrance and exit points of the NP surface for the Au NP (results not shown). The corresponding radial dose profiles (averaged over all solid angles) are presented in figure 3 for an incident 18 MeVu^{-1} C ion
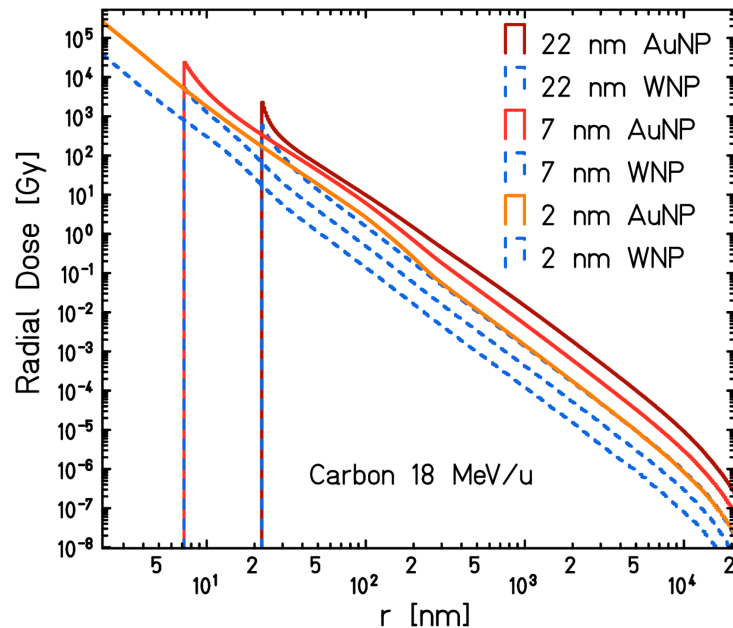
Figure 3. Radial dose profiles for different sizes of isolated Au and water NPs produced by a 18 MeVu^{-1} C ion.

corresponding to a linear energy transfer (LET) in water of ~100 keV/μm. As expected, the absorbed dose in the surrounding medium was always higher for Au NPs. The largest peak dose of > 10^5 Gy was produced with the smallest NP size and respresented an approximately 7-fold increase over the WNP.

The local 2-dimensional (*r,z*) distribution of the *dose difference* around a NP is shown in figures 4(a), (e) and (i) for C, 42 MeVu^{-1}. This is qualitatively representative for all other simulations with p, C, and O in the range 15–204 MeV/u, albeit absolute values varied and were much lower for protons. It can be observed that the additional dose imparted by the Au NP is spherical for the smallest NP but evolves towards two separated 'hot spots' at the NP-medium interface for the larger sizes as a consequence of the high transmission of secondary electrons produced close to the NP surface that contrasts with a significant self-absorption of those generated by primary interactions that take place in the core of the larger NPs. The *DEF* for the isolated NP geometry is depicted in figures 4(c), (g) and (k). It revealed a generally larger enhancement parallel to the ion direction and a more moderate relative dose increase perpendicular to it. This directionality effect was more pronounced for the 7 nm and 22 nm NPs, in agreement with the increased self-absorption described above. Again, the distributions are representative for all energies ≥15 MeVu^{-1} for the three ions studied, with some numerical differences. These differences are better visible in the radial DEF profiles for a series of incident ions, energies, and NP sizes presented in figure 5. The profiles were again obtained by averaging over all solid angles. Different incident ions/energies differed in DEF by 10% to 15 %. The main difference became obvious when changing the NP size: while for the 2 nm case the surface DEF reached around 6–7, for the larger sizes it was 4–5 (7 nm) and ~4 (22 nm). A peak in the curve (up to 20) around 100 nm produced by the smallest NP was greatly reduced for the intermediate size and disappeared for the large NP. Interestingly, the final DEF for larger distances (μm range) becomes uniform close to 11 for all cases. Keeping in mind that (see e.g. figure 3) the absolute radial doses at such a distance for either NP material have decreased by several orders of magnitude, the practical relevance of this result is however very limited. The present radial DEF data are in close agreement with the results that (Tran *et al* 2016) obtained for a 50 nm diameter Au NP and proton radiation using Geant4 / Geant4-DNA.

**3.3. Dose enhancement of a water-embedded NP**

In order to give an idea about the relative importance of the local NP dose increase and the reference ion dose through water, the *absolute dose distributions* simulated in embedded geometry (corresponding to figures 1(c) and (d)) are shown in figures 4(b), (f) and (j) for the three NP sizes. Note that the colour scale is set logarithmic and identical to the one used in the dose difference distributions (figures 4(a), (e) and (i)). If averaged along spherical shells around the NP, the dose deposition qualitatively matched the data presented by Lin *et al* (2015). The 2D *DEF* around the embedded NP is shown in figures 4(d), (h) and (l) using a linear colour scale. The example case of a C ion at 42 MeVu^{-1} is, again, representative for all the combinations examined in the range 15–204 MeVu^{-1} due to the small differences observed. It can be observed that the DEF oscillates around 1 at the z axis, where the dose imparted in pure water (corresponding to the ion track
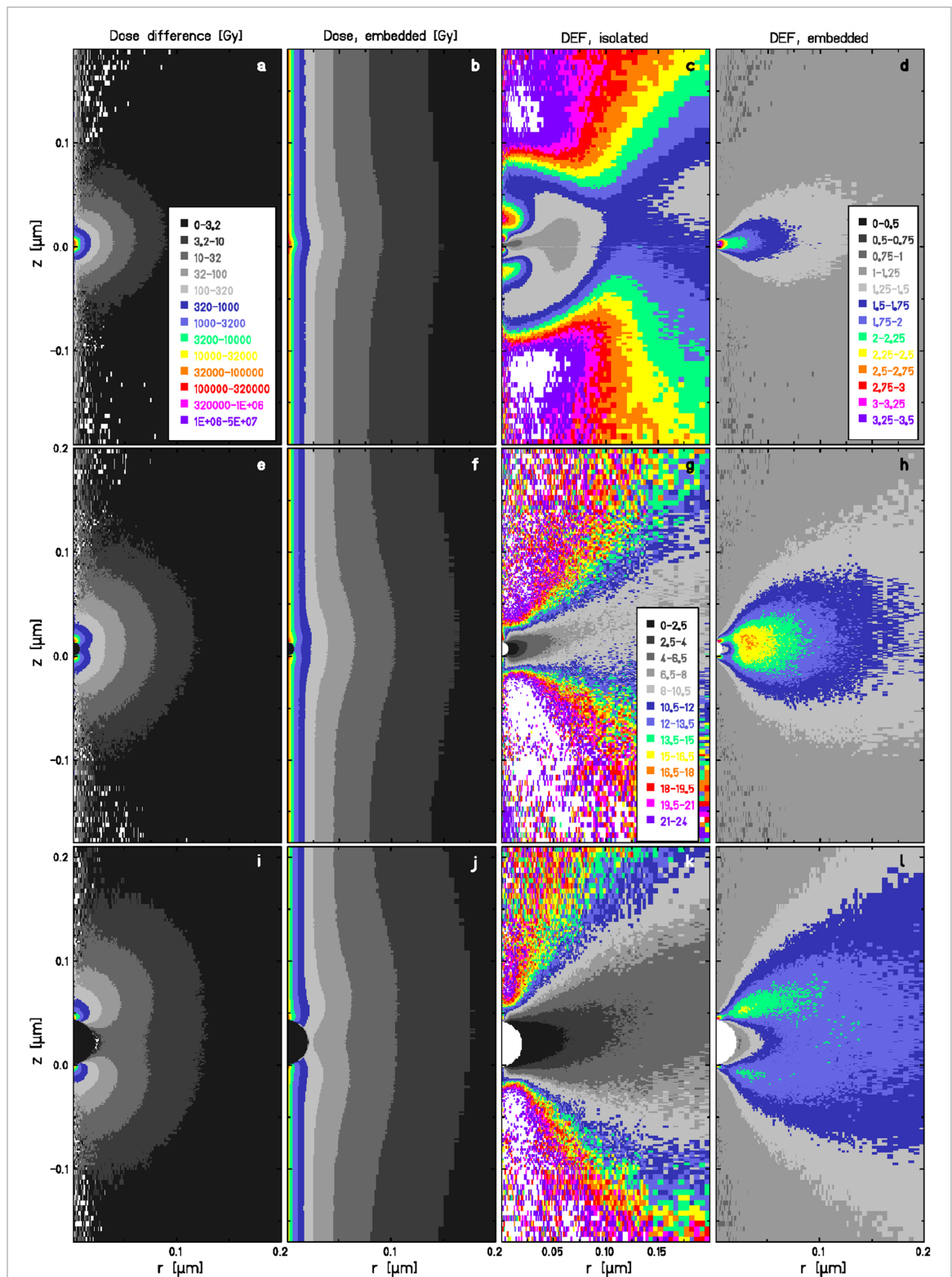
Figure 4. Nanoscale distribution in perpendicular (*r*) and longitudinal (*z*) direction of (left, a,e,i) dose difference, (centre-left, b,f,j) absorbed dose of a water-embedded NP, and dose enhancement factor in (centre-right, c,g,k) isolated and (right, d,h,l) embedded geometry for 42 MeVu^{-1} C ions. NPs have a radius *R* of: 2 nm (top row, a–d), 7 nm (centre, e–h), and 22 nm (bottom row, i–l). The ion path is along the *z*-axis in positive direction with the NP located at $0 \leq z \leq 2$ R. Note that the colour scale for the dose values (left) is logarithmic (each colour step denoting a factor $\sqrt{10}$) and is identical for all cases. Dose distributions were calculated as the average over $2 \cdot 10^6$ to $5 \cdot 10^8$ ion track histories, but nevertheless some statistical noise remains.

core) is already very high and, therefore, dominates the combined dose. The maximum DEF was generally obtained perpendicular to the ion track at the NP location or with a small shift in forward direction and described a torus ('doughnut') centred upon the ion track for all of the cases investigated here. The distance of this DEF maximum depended on the NP size in a way similar to the isolated NP geometry: for the 2 nm radius NP, the DEF peak of ~3.4–3.9 was found 1 nm from the NP surface, while for the larger NPs it was
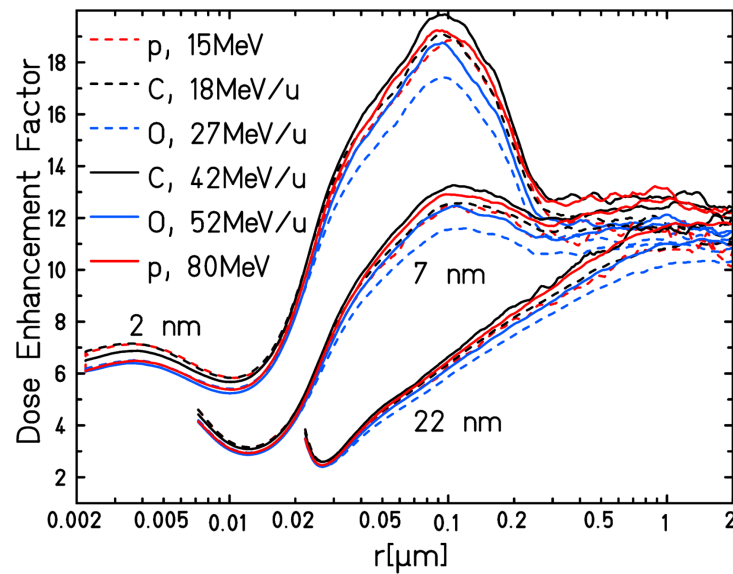
Figure 5. Radially scored DEF of isolated Au/water NPs for different combinations of incident radiation (15–80 MeVu^{-1}) and size (radius 2–22 nm).
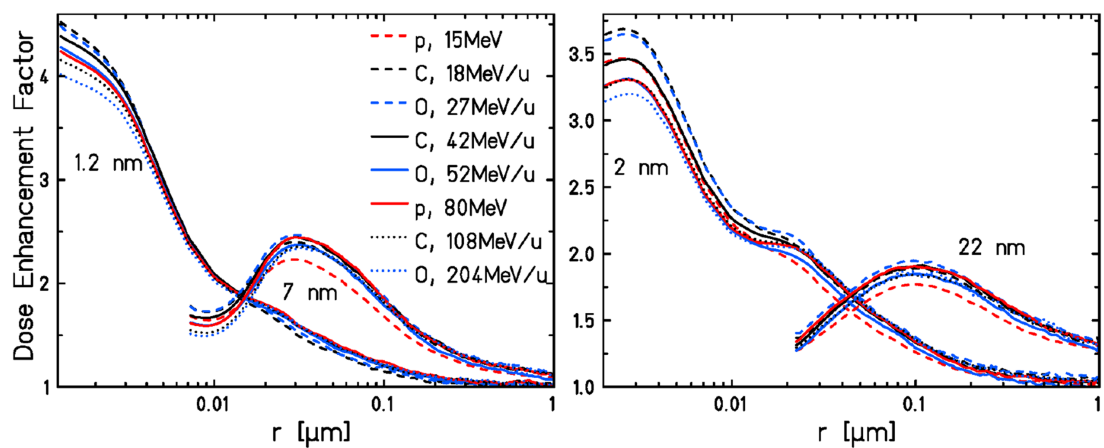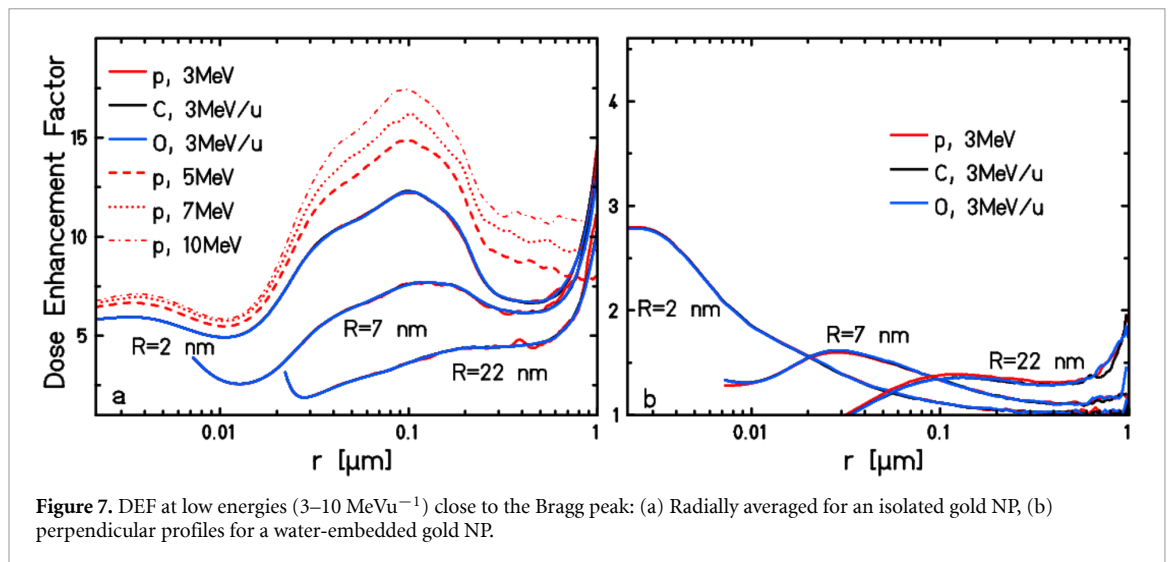

Figure 6. Perpendicular profiles of the DEF in embedded geometry for different combinations of incident radiation (15–200 MeV/u) and NP size (radius of 1.2–22 nm). *r* refers to the distance from the NP centre. Data were averaged over a number of primary histories varying between 10^5 and $5 \cdot 10^8$ depending on ion LET and NP presence/size.

broader and located further away. This obviously implies that for the larger NPs, a substantially larger volume of surrounding material is covered by a significant DEF (around 2.4 or 1.8, respectively), however this DEF applies to a lower absolute radial dose. An overview of the DEF profiles as calculated perpendicular to the ion path at the height of the NP (averaged over $0 \leq z \leq 2$ R) can be seen in figure 6. Variation of the incident energy in the range 15–204 MeVu^{-1} led to slight changes consisting in a lowered DEF at the NP-water interface for increasing $E/A \propto \gamma^2 v^2$ (where E denotes the projectile's kinetic energy, A its mass number, v its velocity and γ is the Lorentz term). (The lowest energy of 15 MeV represents an outlier, probably due to an increased energy loss in the simulation geometry—this is discussed below. For the 22 nm case, the spread at the surface is much compressed and barely appreciated in the figure.) Absolute DEF values are markedly lower than in the isolated geometry, evidencing the fact that the continued ion track in water itself (and the corresponding build-up dose) produces local doses in the same order of magnitude as a high-Z NP. This is of critical importance when assessing the overall enhancement effect in a realistic environment. The total dose deposited in the simulation volume by the gold NP amounts to between 100.5 % and < 104 % (1.2 nm vs. 22 nm size) of the one deposited by a water NP.

3.4. Special considerations

In addition to the initial simulations for energies from 15 MeVu^{-1} upwards, where no major trends could be observed with LET and/or particle E/A as discussed in the previous sections, the situation at ion energies close to the Bragg peak was examined. Note that for the volumes chosen, none of the ions will stop inside the

Figure 7. DEF at low energies (3–10 MeVu^{-1}) close to the Bragg peak: (a) Radially averaged for an isolated gold NP, (b) perpendicular profiles for a water-embedded gold NP.

simulation geometry. However, given the low particle energies and elevated stopping powers (and unlike the previous cases), track segment conditions cannot be assumed any more. A clear decrease of the dose enhancement factor can be seen in figures 7(a) and (b) in both the isolated and embedded NP geometry. This break-down is likely related to the rather flat behaviour of the ion-Au ionization cross sections with energy which is in contrast to a steeper shape that peaks at very low energies for water. This is reflected in the stopping power values as a less pronounced Bragg peak in gold compared to water. Thus, the high relative particle energy loss within the simulation geometry makes these results not directly comparable to the previous ones. Independently, the present results suggest a lower efficiency of gold NP radioenhancement at the low particle energies close to the track end, i.e. in conditions usually found in the target region of therapeutic irradiations. An increased enhancement at high LET values—this has been inferred from some biological experiments (Li *et al* 2016)—is therefore not backed by the dose distributions found and would be contrary to the physical effects described here.

After reporting the local physical dose enhancement caused by the simplest (and 'optimal') case of a NP centrally hit by a proton or heavy ion, some particular variations are studied in the following. Figure 8 depicts the influence on the DEF in embedded geometry of the exact distance *d* from the NP centre where the ion traverses it, taking the 7 nm size as an example. It can be seen that the differences found—mainly a slight shift of the maximum DEF towards the NP—were quite moderate and increased only for hits very close to the NP border. Note that the DEF thus obtained was considerably larger than the one tentatively approximated by scaling the original result (centred case) by the path length *l* travelled through the gold NP, i.e. $(\text{DEF}_{\text{central hit}} - 1) \cdot l/2\,R + 1$. The radial DEF obtained in section 3.3 therefore constituted an upper boundary for the enhancement by a random hit but remained numerically close to the average realistic situation. An equivalent result was obtained for the other NP sizes and radiation qualities. Relative to the central hit, the relatively small decrease of the DEF can be explained by the importance of the 'hot spots' caused by the ion's entrance and exit spots and an only moderate influence of the path length in (or areal density of) gold.

As an extreme case of the non-central incidence, an ion penetrating the medium outside the NP but close to its surface was also investigated. In this way, the indirect physical effect obtained exclusively by secondary electrons subsequently reaching the NP was simulated, thus exploring one of the alternative mechanisms proposed e.g. in Lacombe *et al* (2017). The results for a C 42 MeVu^{-1} ion and the 7 nm radius NP are included in figure 8. No dose enhancement could be seen when there was no direct traversal, instead a decrease in the locally deposited dose appeared immediately when 'missing' the NP by as little as 0.1 nm. This holds true for all of the several combinations of ion species, incident particle energy (up to 400 MeVu^{-1}), and NP size tested (results not shown). In agreement with the DEF profiles presented, the corresponding 2D DEF distributions are dominated by a local minimum similar in size to the NP and surrounded by a DEF of 1. This result clearly indicates that primary ion-NP interactions are necessary for producing a physical enhancement effect: secondary electrons are obviously not sufficient. For them, the high-Z NP acts as a nano-scale shielding element. This is in line with an earlier prediction (Martínez-Rovira and Prezado 2015) of a considerably reduced DEF for Au and Gd nanoparticles when increasing the field size to exceed the NP diameter.
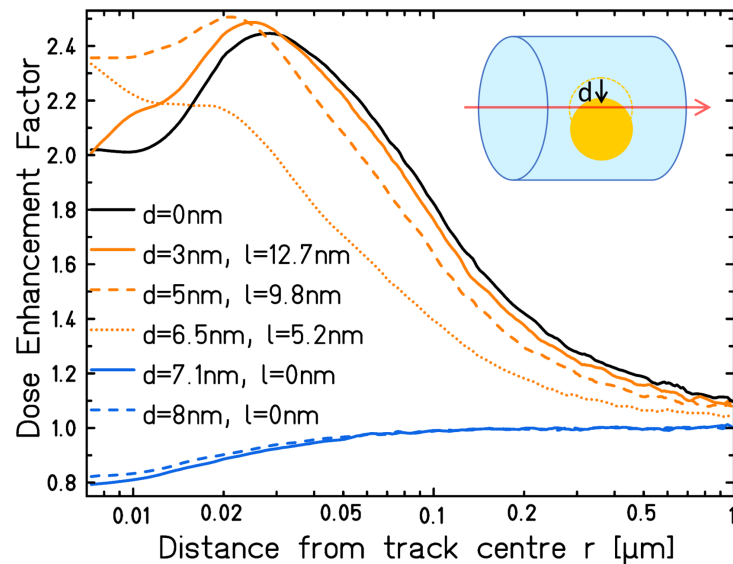
Figure 8. Perpendicular profiles of the DEF in embedded geometry when moving the 7 nm gold NP a distance *d* from the ion track centre, both within and outside of the NP. *l* denotes the path length through gold in either case.
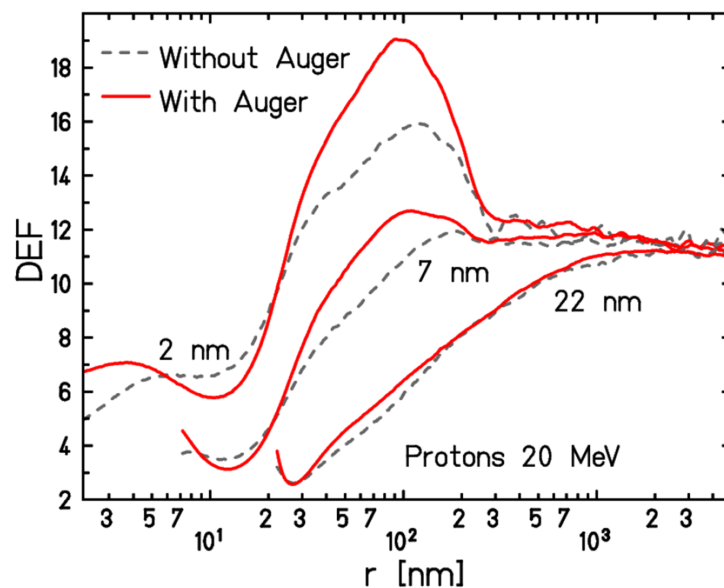
Figure 9. Radial DEF of isolated Au/water NPs when including or excluding Auger electron contributions for a 20 MeV proton beam.

Finally, the contribution of the different depth 'layers' of an embedded gold NP was examined. Even if the presence of absorption within the NP might suggest that a larger amount of metal is counterproductive for dose enhancement, this is not the case. Simulations have been carried out with spherical shells (outer radius of 7 nm and 22 nm), and no critical thickness of such a shell could be determined. Instead, the entire volume contributes progressively to the dose enhancement in the surrounding medium and especially perpendicular to the ion track (see Supplementary material available online at stacks.iop.org/PMB/65/075008/mmedia). A longer path in z-direction through the gold is thus found to be essential to increase the probabilities of inelastic events inside the NP and thus to produce abundant secondary electrons, a portion of which (notably the higher-energy ones) will escape the gold and deliver an additional dose to the surrounding medium.

As Auger emissions from the NP material are sometimes discussed as a source of extra secondary electrons and, hence, dose, we include a quantitative comparison to the dose deposition around the NP with the full Monte Carlo model but suppressing Auger electron generation. Figure 9 depicts the impact of Auger electron inclusion in the simulation in isolated geometry: the maximum dose enhancement factor increased by 19.4% (6.4%) for 2 nm (7 nm) NPs when Auger contributions were accounted for whereas it improved

the value on the slope by up to 13.1% for 22 nm NPs. In all cases, the difference was appreciated most at 50–100 nm distance from the NP centre. As can be seen, Auger processes do play a partial role in physical dose enhancement. This differs from what has been found in the case of X-rays (McMahon *et al* 2011), where Auger electron cascades constitute the main contribution of the dose deposition around the NP.

4. Discussion

The characteristical nano-scale dose enhancement of different sizes of gold NPs under ion irradiation was compared in two different geometries using the TRAX code. The authors want to stress that in the case of ion radiation, the selection of the simulation geometry where the primary interactions take place has a huge influence on the numerical dose enhancement values obtained, with an increase up to a factor 14 (isolated/embedded) close to 100 nm in the 2 nm size and dose enhancement stabilizing at 10–12 for longer distances in the isolated case, whereas it approaches 1 for the embedded geometry. This has however to be interpreted carefully due to the scarce 'real-life' relevance of a scenario where exclusively the NP is traversed. As soon as the high background dose in water around the ion track is considered, only the embedded results apply. Furthermore, when considering the realistic dose increase over the entire biological target (i.e. water) volume simulated here, a maximum of a few percent ($< 4\%$) were never exceeded if a NP was actually hit by the primary particle, and for most combinations and particularly the 1.2 nm and 2 nm sizes, lower values around 1.5% were attained. With this as a starting point, a subsequent approach to translate the physical effect (or even the track chemistry following, as in Boscolo (2018)) into biological damage in the nuclear DNA, similar to existing work (Lin *et al* 2015, Sotiropoulos *et al* 2017, Tran *et al* 2016) is not expected to give a relevant biological enhancement. In this sense, the exact mechanism for sensitization *in vivo* and *in vitro* remains unclear, but some interesting aspects of the dose enhancement are discussed in the following.

Although the radial dose with and without a Au NP depends on the incident ion (particle type, LET), no ion species effect or LET effect was discerned in the present dose enhancement factors. This is in accordance with existing theoretical data for protons (Lin *et al* 2014, Tran *et al* 2016), expanding them to much higher linear energy transfers. At distances close to the NP, the DEFs display a tendency to higher values for slower ions which is explained by the large quantity of additional short-ranged secondary electrons produced under these conditions. In general, the fact that the only mild tendency found was with particle E/A, i.e. velocity, indicates a strong dependence on the secondary electron spectrum and associated range; this also plays a crucial role in the observed self-absorption which is especially pronounced for the low and medium energy secondaries.

Since no pronounced energy or LET dependence was obtained, the DEF behaviour at different distances and for different NP sizes stays valid in mixed fields with the notable exception of the Bragg peak / stopping contribution itself for which a decrease in dose enhancement is predicted according to figure 7. The simulations do therefore not support the LET-dependence (larger enhancement at Bragg peak energies) sometimes seen in experiments (Li *et al* 2016) and do not suggest any beneficial influence on the peak-to-plateau dose ratio.

Gold NPs designed for biological studies and ultimately radiotherapy enhancement purposes are generally furnished with an appropriate organic coating in order to improve cell internalization and biocompatibility. The size dependence observed here implies a vital importance of the coating for very small NPs (around a few nm). A large part of the extra dose within a few nm of the Au NP will actually be deposited in the coating material, not the surrounding target, so that a thicker coating could effectively prevent biological damage (depending on its density, composition, hydration etc), in agreement with *in vitro* experiments with plasmids from Xiao *et al* (2011). For example, when excluding a 5 nm margin around the C 42 MeVu^{-1}-irradiated NP for assuming that it contains no sensitive material, the maximum DEF observed in embedded geometry drops to 2.5–2.6 (2.4–2.6) for the 1.2 nm (2 nm) size and global DEF drops from 1.007 (1.023) to 0.997 (1.012). In contrast, maximum DEF is not affected for the two larger sizes and the global DEF changes only slightly. Dedicated analysis on the influence of the coating can be found in Haume *et al* (2018) and Hespeels *et al* (2019b). Also the cellular localization is more relevant for very small NPs since only nearby structures are affected, but a high enhancement could be achieved in case of successful nuclear targeting. At the same time, the dose enhancement effect of larger NPs (our examples ≥ 7 nm radius) has a considerably longer range so that more independence from these factors can be expected. With regard to the effects in a biological absorber, and considering the usual localization of NPs in the cytoplasm (see e.g. Brun and Sicard-Roselli (2016)), medium-range effects (thus medium-sized NPs) seem preferable to a stronger interface dose increase.

The non-spherical shape of enhancement distributions is generally ignored by previous simulation efforts, maybe due to the fact that an accurate low energy electron model (cross sections) in the metal is necessary (Sakata *et al* 2018) in order to generate and follow the secondaries producing part of the

directional effect. When it comes to biological endpoints, it will however further increase the nanoscale inhomogeneity (local dose peaks) and can be assumed to thereby increase the biological effectiveness.

Our calculations indicate an absence of any indirect physical effect; even a shielding effect is observed if the proton or ion misses the Au target by only 1 Å. Thus, if a direct ion-NP hit is crucial, the probability of such an event under realistic ion beam therapy conditions and feasible NP concentrations has important implications for the total effect that can be expected at the cellular scale. A simple estimation using typical *in vitro* conditions is made in the following: a HeLa cell is assumed to have a surface of approximately 850 μm^2 in a monolayer culture and internalizes about $5 \cdot 10^5$ gold NPs after incubation with a 0.5mM NP suspension (Bolsa Ferruz 2017). For NPs with a radius of 1.2 nm, this equates to a total Au 'cross section' area of $\sim 2.3 \mu m^2$ or a ~0.25% of the cell area. When exposed to a fraction of 2 Gy in a scanned heavy ion beam of 100 keV/μm, the corresponding fluence of $\sim 1.2 \cdot 10^7/cm^2$ would result in an expected value of only 0.22 NP hits per cell. At the same concentration of nanoparticles per volume and supposing identical internalization, a larger NP size would offer a larger cross section area perpendicular to the beam and thus increase the number of hits to 8.7 (86) per cell or 8.5% (84%) of ion tracks for the 7 nm (22 nm) NP, thereby reaching a non-negligible contribution in the % range for the largest NP in a *homogeneous* absorber. Note, however, that for a radius of 22 nm this would exceed the generally accepted maximum of 1% (weight) gold concentration, so that the use of similarly large NP sizes is generally associated to a lower internalized concentration. On the contrary, if we keep the gold material concentration constant with respect to the smallest NP, the hits expected per cell drop down to 0.0014 for the 22 nm NP, leaving the smallest size as the best choice in the supposed homogeneous absorber in line with the results of Lin *et al* (2015).

Observations of NP clustering upon cell uptake have recently prompted studies about the effect of clustering on dose deposition or radiolysis (Villagomez-Bernabe and Currell 2019, Peukert *et al* 2019, Rudek *et al* 2019). Their results for proton/ion beams show a decrease of DEF for clustered NPs compared to dispersed ones (Peukert *et al* 2019, Rudek *et al* 2019) and increased OH$^\bullet$ G-values in the clustered case (Rudek *et al* 2019). One should keep in mind that for typical heavy ion irradiations, the separation between individual tracks is rather large (one ion track per 10 μm^2 for fluences of $10^7/cm^2$) and accordingly the probability for two tracks to hit two contiguous (clustered) NPs is vanishingly small. Still, one ion can interact with one NP in proximity of a second one which is not crossed by any primary. According to figure 8, this is expected to result in a certain absorption effect for very short distances and can explain the DEF reduction (Peukert *et al* 2019, Rudek *et al* 2019) mentioned before. To estimate the net enhancement effect in such a situation, a few simple simulations were run with clustered NPs in a broad field (thought to best represent the statistical average over ion tracks inciding at random positions). One, two or three NPs ($R = 17.5$ nm) separated by about 20 nm of water yielded a global DEF, over a volume of 0.05 μm^3, of up to 1.003. This is in good agreement with the concentration-dependent findings of Rudek *et al* (2019) for C ions and shows no significant deviation from additive behaviour. The fact that the globally scored DEF becomes so tiny in a broad field further underlines the large sensitivity to simulation geometry and in consequence the importance of employing realistic set-ups in modelling studies.

5. Conclusions

We have examined the nano-scale dose enhancement characteristics of gold NPs under ion irradiation in full detail and have found large local dose enhancement factors of up to 20 (4.6) for isolated (embedded) NPs. By simulating three different ion species (protons, C ions and O ions), a possible dependency of dose enhancement on linear energy transfer, which is sometimes suggested, would be clearly uncovered but is not supported by our results. An important related aspect is however the Bragg peak (stopping region of the incident ions) where we have found a much suppressed dose enhancement for all ion species examined, which questions the generally desired improvement of peak-to-entrance dose ratio. Furthermore, by moving the NP laterally with respect to the incident ion, we have ruled out any indirect physical effect (i.d. dose enhancement relying only on secondary electrons' interactions with the NP) for ion irradiation. We have also provided data showing that the specific impact of Auger electrons is moderate but not negligible and localizes in the range of ~30–150 nm from the centre of the NP. The local 2D distributions of absorbed dose, dose difference or dose enhancement factor in combination with secondary emission spectra have allowed us to explore the (self-)absorption in the metal which affects primarily secondary electron energies between a few eV and 200 eV —and thus the enhancement close to the NP surface—and becomes increasingly important as the NP size grows above few nm (radius).

The enhancement range dependence with NP size we obtained suggests that especially the balance between metal core size and coating dimensions is critical and should be selected depending on the expected cellular localization (distance from sensitive target). A thicker coating layer will generally require a larger gold core so that the extra dose effectively reaches the biological medium. In some biological experiments, some

additional tenths in sensitizer enhancement ratio or RBE increase or some tens of percent improvement of complete tumour regression have been observed (for a summary, see Peukert *et al* (2018)). However, globally the present results do not suggest a physical enhancement origin of these biological endpoints. On the one hand, as discussed in detail above, the volumes covered by an enhancement in combination with the known cellular localization outside the nucleus and the small probability of a direct hit do clearly not support a sufficiently pronounced overall effect on a cellular scale. On the other hand, the trends predicted by the present calculations are not generally reflected in—or are sometimes even contradictory to—the biological sensitization effects described. We therefore point out that a truly biological pathway of action is more likely the main mechanism behind previously observed *in vitro* and *in vivo* sensitization to proton or ion irradiation by gold nanoparticles, as several authors have proposed (Jain *et al* 2011). Especially oxidative stress (Butterworth *et al* 2013) of the mitochondria (Pan *et al* 2009), and particularly depolarization (Kam and Banati 2013, Kam *et al* 2013), seem to play important roles that could work synergistically together and amplify with radiation towards a depletion of the available antioxidants. For gold NPs, a biological pathway triggered by gold ions depending on the NP internalization route in the cytoplasm and leading to an endogenous reactive oxygen species production (Penninckx *et al* 2018) could indeed be at work with and without irradiation. Still, the large differences observed experimentally in endpoints as cell survival, tumour progression or animal overall survival after irradiation in presence of high Z metal nanoparticles, indicate that those mechanisms are by no means universal and in their absence the purely physical effects do not prove decisive.

Acknowledgements

ORCID iDs

M C Fuss ⦿ https://orcid.org/0000-0001-5332-6491
D Boscolo ⦿ https://orcid.org/0000-0001-5709-4472
M Durante ⦿ https://orcid.org/0000-0002-4615-553X
E Scifoni ⦿ https://orcid.org/0000-0003-1851-5152

References

Bolsa Ferruz M 2017 Oxygen effect in medical ion beam radiation combined with nanoparticles *PhD thesis* Université de Paris Saclay (www.theses.fr/2017SACLS476)

Boscolo D 2018 Nanoscale insights on hypoxia radiosensitization with ion beams *PhD thesis* TU Darmstadt (https://tuprints.ulb.tu-darmstadt.de/8159/)

Boscolo D, Krämer M, Durante M, Fuss M C and Scifoni E 2018 TRAX-CHEM: A pre-chemical and chemical stage extension of the particle track structure code TRAX in water targets *Chem. Phys. Lett.* **698** 11–18

Boscolo D, Krämer M, Fuss M C, Durante M and Scifoni E 2020 Impact of target oxygenation on the chemical track evolution of ion and electron radiation *Int. J. Mol. Sci.* **21** 424

Brun E and Sicard-Roselli C 2016 Actual questions raised by nanoparticle radiosensitization *Radiat. Phys. Chem.* **128** 134–42

Butterworth K T, McMahon S J, Taggart L E and Prise K M 2013 Radiosensitization by gold nanoparticles: effective at megavoltage energies and potential role of oxidative stress *Transl. Cancer Res.* **2** 269–79

Chitrani D B, Jelveh S, Jalali F, van Prooijen M, Allen C, Bristow R G, Hill R P and Jaffray D A 2010 Gold nanoparticles as radiation sensitizers in cancer therapy *Radiat. Res.* **173** 719–28

Conde J, Dias J T, Grazú V, Moros M, Baptista P V and de la Fuente J M 2014 Revisiting 30 years of biofunctionalization and surface chemistry of inorganic nanoparticles for nanomedicine *Frontiers Chem.* **2** 48

Cui L, Tse K, Zahedia P, Harding S M, Zafarana G, Jaffray D A, Bristow R G and Allen C 2014 Hypoxia and cellular localization influence the radiosensitizing effect of gold nanoparticles (AuNPs) in breast cancer cells *Radiat. Res.* **182** 475–88

Delorme R, Taupin F, Flaender M, Ravanat J L, Champion C, Agelou M and Elleaume H 2017 Comparison of gadolinium nanoparticles and molecular contrast agents for radiation therapy-enhancement *Med. Phys.* **44** 5949–60

Dollinger G 2011 Comment on "Therapeutic application of metallic nanoparticles combined with particle-induced x-ray emission effect" *Nanotechnology* **22** 248001

Ferrero V, Visonà G, Dalmasso F, Gobbato A, Cerello P, Strigari L, Visentin S and Attili A 2017 Targeted dose enhancement in radiotherapy for breast cancer using gold nanoparticles, part 1: A radiobiological model study *Med. Phys.* **44** 1983–92

Geng F, Song K, Xing J Z, Yuan C, Yan S, Yang Q, Chen J and Kong B 2011 Thio-glucose bound gold nanoparticles enhance radio-cytotoxic targeting of ovarian cancer *Nanotechnology* **22** 285101

Hainfeld J F, Slatkin D N and Smilowitz H M 2004 The use of gold nanoparticles to enhance radiotherapy in mice *Phys. Med. Biol.* **49** N309

Haume K, de Vera P, Verkhovtsev A, Surdutovich E, Mason N J and Solov'yov A V 2018 Transport of secondary electrons through coatings of ion-irradiated metallic nanoparticles *Eur. Phys. J. D* **72** 116

Herold D M, Das I J, Iyer R V and Chapman J D 2000 Gold microspheres: a selective technique for producing biologically effective dose enhancement *Int. J. Radiat. Biol.* **76** 1357–64

Hespeels F, Heuskin A C, Scifoni E, Krämer M and Lucas S 2017 Backscattered electron emission after proton impact on carbon and gold films: Experiments and simulations *Nucl. Instrum. Meth. B* **401** 8–17

Hespeels F, Heuskin A C, Tabarrant T, Scifoni E, Krämer M, Chêne G, Strivay D and Lucas S 2019b Backscattered electron emission after proton impact on gold nanoparticles with and without polymer shell coating *Phys. Med. Biol.* **64** 125007

Hespeels F, Lucas S, Tabarrant T, Scifoni E, Krämer M, Chêne G, Strivay D, Tran H N and Heuskin A C 2019a Experimental measurements validate the use of the binary encounter approximation model to accurately compute proton induced dose and radiolysis enhancement from gold nanoparticles *Phys. Med. Biol.* **64** 065014

Jain S *et al* 2011 Cell-specific radiosensitization by gold nanoparticles at megavoltage radiation energies *Int. J. Radiat. Oncol. Biol. Phys.* **79** 531–9

Jeynes J C G, Merchant M J, Spindler A, Wera A C and Kirkby K J 2014 Investigation of gold nanoparticle radiosensitization mechanisms using a free radical scavenger and protons of different energies *Phys. Med. Biol.* **59** 6431

Jones B, Krishnan S and Cho S H 2010 Estimation of microscopic dose enhancement factor around gold nanoparticles by Monte Carlo calculations *Med. Phys.* **37** 3809

Kam W W Y and Banati R B 2013 Effects of ionizing radiation on mitochondria *Free Rad. Biol. Med.* **65** 607–19

Kam W W Y, McNamara A L, Lake V, Banos C, Davies J B, Kuncic Z and Banati R B 2013 Predicted ionisation in mitochondria and observed acute changes in the mitochondrial transcriptome after gamma irradiation: A Monte Carlo simulation and quantitative PCR study *Mitochondrion* **13** 736–42

Kim J K, Seo S J, Kim H T, Kim K H, Chung M H, Kim K R and Ye S J 2012 Enhanced proton treatment in mouse tumors through proton irradiated nanoradiator effects on metallic nanoparticles *Phys. Med. Biol.* **57** 8309–23

Kim J K, Seo S J, Kim K H, Kim T J, Chung M H, Kim K R and Yang T K 2010 Therapeutic application of metallic nanoparticles combined with particle-induced x-ray emission effect *Nanotechnology* **21** 425102

Krämer M and Kraft G 1994 Calculations of heavy-ion track structure *Radiat. Environ. Biophys.* **33** 91–109

Kuncic Z and Lacombe S 2018 Nanoparticle radio-enhancement: principles, progress and application to cancer treatment *Phys. Med. Biol.* **63** 02TR01

Lacombe S, Porcel E and Scifoni E 2017 Particle therapy and nanomedicine: state of the art and research perspectives *Cancer Nanotechnol.* **8** 9

Lechtman E, Chattopadhyay N, Cai Z, Mashouf S, Reilly R and Pignol J P 2011 Implications on clinical scenario of gold nanoparticle radiosensitization in regards to photon energy, nanoparticle size, concentration and location *Phys. Med. Biol.* **56** 4631

Li S *et al* 2016 LET-dependent radiosensitization effects of gold nanoparticles for proton irradiation *Nanotechnology* **27** 455101

Lin Y, McMahon S, Paganetti H and Schuemann J 2015 Biological modeling of gold nanoparticle enhanced radiotherapy for proton therapy *Phys. Med. Biol.* **60** 4149–68

Lin Y, McMahon S, Scarpelli M, Paganetti H and Schuemann J 2014 Comparing gold nano-particle enhanced radiotherapy with protons, megavoltage photons and kilovoltage photons: a Monte Carlo simulation *Phys. Med. Biol.* **59** 7675–89

Martínez-Rovira I and Prezado Y 2015 Evaluation of the local dose enhancement in the combination of proton therapy and nanoparticles *Med. Phys.* **42** 6703–10

Matsudaira H, Ueno A M and Furuno I 1980 Iodine contrast medium sensitizes cultured mammalian cells to X rays but not to γ rays *Radiat. Research* **84** 144–8

McMahon S J *et al* 2011 Biological consequences of nanoscale energy deposition near irradiated heavy atom nanparticles *Sci. Rep.* **1** 18

Montenegro M, Nahar S N, Pradhan A K, Huang K and Yu Y 2009 Monte Carlo simulations and atomic calculations for auger processes in biomedical nanotheranostics *J. Phys. Chem.* A **113** 12364–9

Pan Y, Leifert A, Ruau D, Neuss S, Bornemann J, Schmid G, Brandau W, Simon U and Jahnen-Dechent W 2009 Gold nanoparticles of diameter 1.4 nm trigger necrosis by oxidative stress and mitochondrial damage *Small* **5** 2067–76

Penninckx S, Heuskin A C, Michiels C and Lucas S 2018 The role of thioredoxin reductase in gold nanoparticle radiosensitization effects *Nanomedicine* **13** 2917–37

Peukert D, Kempson I, Douglass M and Bezak E 2018 Metallic nanoparticle radiosensitisation of ion beam radiotherapy: A review *Phys. Medica* **47** 121–8

Peukert D, Kempson I, Douglass M and Bezak E 2019 Gold nanoparticle enhanced proton therapy: Monte Carlo modeling of reactive species' distributions around a gold nanoparticle and the effects of nanoparticle proximity and clustering *Int. J. Mol. Sci.* **20** 4280

Polf J C, Bronk L F, Driessen W H P, Arap W, Pasquali R and Gillin M 2011 Enhanced relative biological effectiveness of proton radiotherapy in tumor cells with internalized gold nanoparticles *Appl. Phys. Lett.* **98** 193702

Rudek B, McNamara A, Ramos-Mendez J, Byrne H, Kuncic Z and Schuemann J 2019 Radio-enhancement by gold nanoparticles and their impact on water radiolysis for x-ray, proton and carbon-ion beams *Phys. Med. Biol.* **64** 175005

Sakata D *et al* 2018 Geant4-DNA track-structure simulations for gold nanoparticles: the importance of electron discrete models in nanometer volume *Med. Phys.* **45** 2230–42

Sotiropoulos M, Henthorn N T, Warmenhoven J W, Mackay R I, Kirkby K J and Merchant M J 2017 Modelling direct DNA damage for gold nanoparticle enhanced proton therapy *Nanoscale* **9** 18413–22

Tran H N *et al* 2016 Geant4 Monte Carlo simulation of absorbed dose and radiolysis yields enhancement from a gold nanoparticle under mev proton irradiation *Nucl. Instrum. Meth. Phys. Res. B* **373** 126–39

Verkhovtsev A V, Korol A V and Solov'yov A V 2015 Revealing the mechanism of the low-energy electron yield enhancement from sensitizing nanoparticles *Phys. Rev. Lett.* **114** 063401

Villagomez-Bernabe B and Currell F J 2019 Physical radiation enhancement effects around clinically relevant clusters of nanoagents in biological systems *Sci. Rep.* **9** 8156

Wälzlein C, Krämer M, Scifoni E and Durante M 2014a Advancing the modeling in particle therapy: from track structure to treatment planning *Appl. Radiat. Isot.* **83** 171–6

Wälzlein C, Scifoni E, Krämer M and Durante M 2014b Simulations of dose enhancement for heavy atom nanoparticles irradiated by protons *Phys. Med. Biol.* **59** 1141–458

Williart A, Muñoz A, Boscolo D, Krämer M and García G 2019 Study on tl-204 simultaneous electron and photon emission spectra and their interaction with gold absorbers. Experimental results and Monte Carlo simulations *Nucl. Instrum. Meth.* A **927** 435–42

Xiao F, Zheng Y, CLoutier P, He Y, Hunting D and Sanche L 2011 On the role of low-energy electrons in the radiosensitization of DNA by gold nanoparticles *Nanotechnology* **22** 465101

Xie W Z, Friedland W, Li W B, YLi C, Oeh U, Qiu R, Li J L and Hoeschen C 2015 Simulation on the molecular radiosensitization effect of gold nanoparticles in cells irradiated by x-rays *Phys. Med. Biol.* **60** 6195–6212